Microstructure and carbon storage capacity of hydrated magnesium carbonates synthesized from different sources and conditions

Haoliang Dong[a], Cise Unluer[a], En-Hua Yang[a,*], Fei Jin[b], Abir Al-Tabbaa[b]

[a] School of Civil and Environmental Engineering, Nanyang Technological University, 50 Nanyang Avenue, Singapore 639798, Singapore

[b] Department of Engineering, University of Cambridge, Trumpington Street, Cambridge CB2 1PZ, UK

Abstract

Recently, the mineral carbonation via the reaction of CO_2 with saline aquafers received much attention as one of the most promising ways for geologic CO_2 storage. This paper reports microstructure and carbon storage capacity of hydrated magnesium carbonates (HMCs) synthesized from different sources, *i.e.,* reject brine and commercial $Mg(OH)_2$ slurry, and under different conditions, *i.e.,* pH (8-14) and $Mg(OH)_2$:CO_2 molar ratio (1:1-1:7). Results show that dypingite ($Mg_5(CO_3)_4(OH)_2{\cdot}5H_2O$) is the main phase forming at lower $Mg(OH)_2$:CO_2 ratios. An increase in the $Mg(OH)_2$:CO_2 ratio and/or pH leads to the precipitation of nesquehonite ($MgCO_3{\cdot}3H_2O$). A unique "house of cards" texture, involving formation of the rosette-like dypingite flakes on the surface of nesquehonite needles, is discovered under elevated pH and $Mg(OH)_2$:CO_2 ratios. HMCs synthesized from reject brine exhibit a much higher carbon storage capacity of 82.6% than that produced from the commercial $Mg(OH)_2$ slurry (43.7%).

* Corresponding author. Address: N1-01b-56, 50 Nanyang Avenue, Singapore 639798. Tel.: +65 6790 5291; fax: +65 6791 0676. *E-mail:* ehyang@ntu.edu.sg

Findings from this study advance understanding of mineral recovery from reject brine and the capture and long-term storage of CO_2 in the form of HMCs.

Keywords: *Reject brine; $Mg(OH)_2$; pH; hydrated magnesium carbonates (HMCs); carbon capture and storage*

1. Introduction

Fossil fuels have been the world's primary energy source, providing over 85% of the energy demands worldwide [1-6]. However, nearly 83% of the anthropogenic greenhouse gas (GHG) emissions are coming from combustion and non-fuel uses of fossil fuels [7]. CO_2, which is the main GHG, has caused most of the global warming since it has the highest positive radiative forcing and far more abundant in the atmosphere than other heat-trapping gases [8, 9]. The concentration of CO_2 in the atmosphere has increased ~30% from 325 parts per million (ppm) at the beginning of the industrial era in 1970 to 409.7 ppm in May 2017 measured in Mauna Loa Observatory. Consequently, much attention has been drawn to the carbon management [10-12]. Carbon capture and storage (CCS) provides a feasible way to reduce the build-up of CO_2 in the atmosphere [13, 14]. CCS concept covers broad fields such as ocean, terrestrial, geological, biological and chemical approaches to store CO_2 gas in the long term [15-18], among which mineral carbonation via the reaction of CO_2 with saline aquafers is one of the most promising geologic CO_2 storage options [19-23]. Magnesium-based minerals have attracted great attentions worldwide as they show the potential to sequestrate anthropogenic CO_2 to counterpart the global warming [24-27]. Furthermore, reactive magnesia (MgO) cement has been studied as a potential alternative to the Portland cement due to its ability to sequester significant amount of carbon dioxide (CO_2) and potential to be fully recycled [28-32].

Although the most thermodynamically stable carbonate for magnesium is in the anhydrous form, *i.e.,* magnesite ($MgCO_3$) [33-35], formation of magnesite at the ambient condition is not common. Instead, formation of hydrated magnesium carbonates (HMCs) prevails as Mg^{2+} ions in the solution are highly hydrated [24]. HMCs are a class of magnesium compounds that form in MgO-CO_2-H_2O systems, where the carbonation of magnesium systems generate a variety of phases, including dypingite ($Mg_5(CO_3)_4(OH)_2 \cdot 5H_2O$) [36], hydromagnesite ($Mg_5(CO_3)_4(OH)_2 \cdot 4H_2O$) [37], and nesquehonite ($MgCO_3 \cdot 3H_2O$) [18, 38]. It has been reported that inclusion of HMCs in reactive MgO cement enhances carbonation of the resulting binder [39].

Theoretically, the formation of different phases of HMCs with different morphologies is influenced by temperature, pH and CO_2 partial pressure [24, 40, 41]. Recent experimental studies show that the precipitation of nesquehonite with needle-like morphology in an aqueous solution occurs commonly under ambient conditions [15, 18, 38]. As the reaction temperatures (333-368 K) and pH values increased, needle-like nesquehonite was replaced by hydromagnesite with sheet-like morphology since nesquehonite is widely known to transform to hydromagnesite at temperature above 50°C [40]. Hydromagnesite was reported to form at 120°C and P_{CO2} of 3 bar, which gradually transformed to magnesite within 5-15 hours. However, a further increase of P_{CO2} to 100 bar at 120°C resulted in the direct precipitation of magnesite [24]. The thermal behavior of the synthesized HMCs (*e.g.,* nesquehonite) has been tested through real time in-situ X-ray diffraction (XRD), which indicated that nesquehonite and dypingite remained thermal and structural stable up to 373 K and 435 K, respectively [36, 42]. Under the continued thermal treatment, nesquehonite transited into magnesite which was even thermally stable up to 600 K, while dypingite transited into hydromagnesite at around 570 K, assuring the long-term storage of CO_2. However, the influences of $Mg(OH)_2/CO_2$ molar ratios

and pH on the phases, morphology, and CCS efficiency of HMCs have yet been studied systematically.

Desalination is a process that removes minerals from saline water. In coastal regions such as Singapore where sources of fresh water are limited, desalination provides a feasible option to produce fresh water. However, a high salty waste stream (*i.e.,* reject brine) would be generated as much as the produced desalinated water at the end of the process [43]. Reject brine is a much more complex media because chemicals are often added into the intake seawater (*e.g.,* to precipitate the colloidal particles before running through the ultra-filtration) in the desalination process (Fig. 1). Although many studies have investigated mineral trapping of CO_2 into saline aquafers (*e.g.,* seawater, natural brine, or synthesized $MgCl_2$ solution) [18, 36, 42, 44-46], very few has reported the use of reject brine as the CO_2 reservoir [47] and no study has proposed to use reject brine as the $Mg(OH)_2$ source to synthesize HMCs.

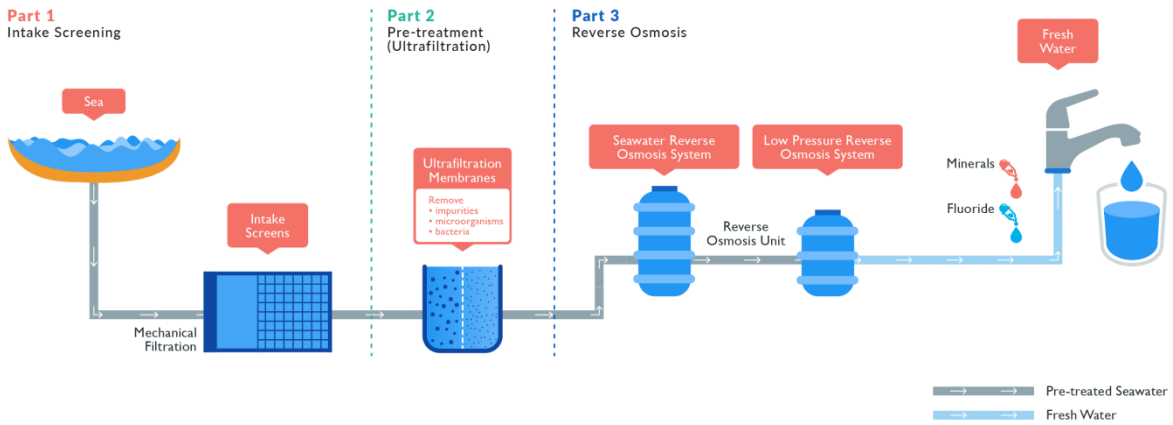

Figure 1 Schematic illustration of the typical process in a reverse osmosis desalination plant [48]

In this paper, influence of key parameters including $Mg(OH)_2$:CO_2 molar ratio, pH, and $Mg(OH)_2$ source on HMCs synthesis were investigated. The resulting HMCs were characterized by means of XRD, scanning electron microscopy (SEM), and thermogravimetric/differential thermal analysis (TG/DTA) to reveal phases, morphology, and CCS efficiency of HMCs synthesized under different conditions. In the following sections, materials and methodologies are presented first, followed by results presentation and discussion.

2. Materials and Methodology

2.1. Materials

Reject brine sample was collected from a local desalination plant which generates 318,500 m^3 desalinated water per day. The sample was filtrated through a 45 μm membrane filter to remove suspended solids before further analysis. An inductively coupled plasma-optical emission spectroscopy (ICP-OES) was used to analyze the chemical composition of reject brine in the current study (Table 1). Analytical grade $Mg(OH)_2$ (92% pure) and analytical grade sodium hydroxide (NaOH) with a purity of 97% were both purchased from VWR Pte Ltd in Singapore. Compressed CO_2 was purchased from Leeden National Oxygen Ltd in Singapore.

Table 1 Chemical composition of reject brine

Element	Cl	Na	SO_4	Mg	K	Ca	Sr	B	Si	Li	P	Al
Concentration (ppm)	65593	13580	4323	1718	846	471	14.6	3.8	3.7	0.3	0.2	0.1

2.2. Methodology

In the first approach, 0.82 g commercially available analytical grade $Mg(OH)_2$ was dissolved into 200 ml ultra-pure water to prepare the $Mg(OH)_2$ slurry. To study the influences of

$Mg(OH)_2/CO_2$ molar ratios and pH on the microstructures of HMCs , three sets of experiments were designed at controlled conditions, *i.e.,* $Mg(OH)_2$:CO_2 molar ratio (1:1-1:7) and pH (8-14). CO_2 was sparged into the slurry at a rate of 100 ml/min at room temperature under pre-determined conditions as follows,

a) pH = 8, $Mg(OH)_2$:CO_2 molar ratio = 1:1 to 1:7
b) pH = 8 to 11, $Mg(OH)_2$:CO_2 molar ratio = 1:1
c) pH = 8 to 11, $Mg(OH)_2$:CO_2 molar ratio = 1:2

In the second approach, $Mg(OH)_2$ was first synthesized from the reject brine via the addition of NaOH at an optimized condition (*i.e.,* NaOH/Mg^{2+} ratio of 2 at 25^{o}C) determined from our previous work [49-51], which results high yield and high purity $Mg(OH)_2$. After which, 0.82 g of synthesized $Mg(OH)_2$ was mixed with 200 ml ultra-pure water. CO_2 was sparged into the slurry at a rate of 100 ml/min at room temperature under controlled condition (*i.e.,* pH = 8, $Mg(OH)_2$:CO_2 molar ratio = 1:1).

A pH/thermometer probe, inserted into reject brine, was used to continuously record the temperature and pH during the experiment. A CO_2 flowmeter was used to monitor and record the volume of CO_2 diffused into the slurry. Once the diffused CO_2 reached the pre-determined value (*i.e.,* calculated based on the designed $Mg(OH)_2$:CO_2 molar ratio), the reaction was terminated. 1M NaOH was added into the slurry continuously to maintain the pH to the designed value since sparging CO_2 lowered the pH of slurry. HMCs were separated from the solution by a centrifuge and washed three times using ultra-pure water. The washed samples were fully dried in an oven at low temperature (*i.e.,* 40°C) to avoid any phase changes, before being ground into powder form. The prepared powder was finally passed through a 125 μm sieve for further microstructural analysis.

ICP-OES (PerkinElmer Optima DV2000) was employed to measure the chemical composition of the reject brine before and after the reactions. The XRD (Bruker D8 Advance) diffractagrams of the synthesized HMCs were recorded from 5° to 70° at 0.02°/step with a CuKα radiation at 40 kV and 40 mA. The morphology of the synthesized HMCs was investigated by a field emission SEM (JSM-7600F). TG/DTA (PyrisDiamond 4000) of the synthesized HMCs was operated at a heating rate of 10°C/min under the air flow condition.

3. Results and Discussion

3.1. Characterization of HMCs synthesized from $Mg(OH)_2$ slurry

3.1.1. Effect of $Mg(OH)_2/CO_2$ molar ratio

Figure 2 shows the FESEM images of all samples obtained under a constant pH of 8 while the $Mg(OH)_2$:CO_2 molar ratio was varied between 1:1 and 1:7. The morphologies of the obtained HMCs dramatically changed with the $Mg(OH)_2$:CO_2 molar ratio. For instance, the rosette-like morphology observed when the $Mg(OH)_2$:CO_2 molar ratio was 1:1 (Fig. 2a), which was eventually replaced by rod-like structures with smooth surfaces when this ratio gradually increased to 1:6 (Figs. 2b-f). The boundaries of these rod-like carbonate phases became clearer with an increase in the $Mg(OH)_2$:CO_2 molar ratio. A further increase in the $Mg(OH)_2$:CO_2 molar ratio to 1:7 revealed the formation of a layer of rosette-like flakes around the original rod-like morphology, producing a “house of cards” texture on the surface [52], as shown in Fig. 2g.

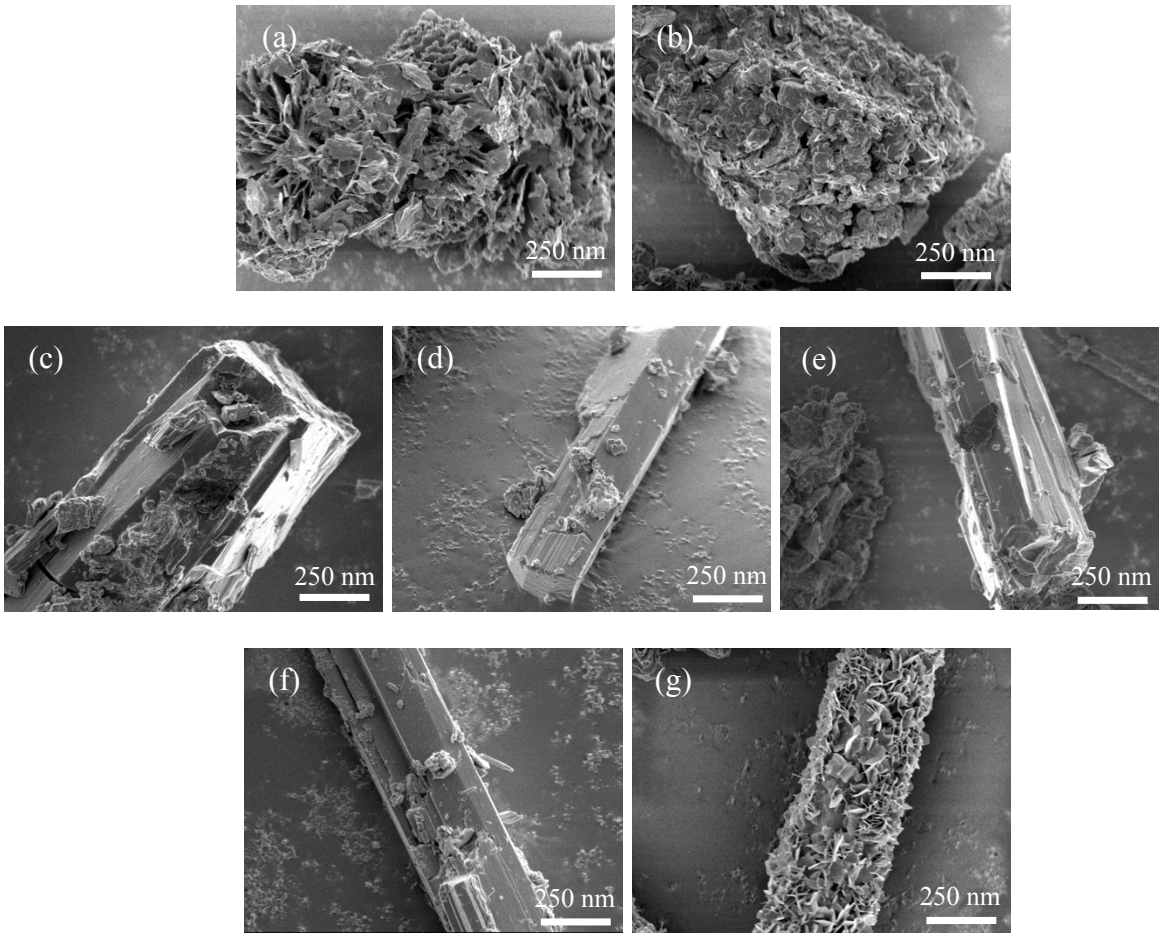

Figure 2 FESEM images of HMCs obtained under a pH of 8 at different $Mg(OH)_2$:CO_2 molar ratios of (a) 1:1, (b) 1:2, (c) 1:3, (d) 1:4, (e) 1:5, (f) 1:6 and (g) 1:7

Fig. 3 indicates the XRD diffractograms of the same set of samples obtained under a pH of 8 at different $Mg(OH)_2$:CO_2 molar ratios. The XRD patterns confirmed that the rosette- and rod-like particles observes in Fig. 2 could be attributed to dypingite and nesquehonite, respectively. These morphological observations were in line with the previous literature [18, 36, 41], where the distinct morphologies of dypingite and nesquehonite were reported. At the $Mg(OH)_2$:CO_2 molar ratio of 1:1, the precipitates consisted of dypingite, uncarbonated brucite and dolomite that was present as an impurity within $Mg(OH)_2$. An increase in the $Mg(OH)_2$:CO_2 molar ratio to 1:2 revealed a reduction in the amount of uncarbonated brucite, resulting in the domination of nesquehonite. These results corresponded well with the chemical composition of different

176 carbonate phases. Accordingly, the abundance of nesquehonite could be associated with the
177 availability of higher amounts of CO_2 introduced into the mix under higher $Mg(OH)_2$:CO_2
178 molar ratios. This is because nesquehonite ($MgCO_3 \cdot 3H_2O$) requires a higher Mg:CO_2 molar
179 ratio of 1:1 than dypingite ($Mg_5(CO_3)_4(OH)_2 \cdot 5(H_2O)$), which can theoretically form at a
180 corresponding ratio of 1:0.8. Further increase of the $Mg(OH)_2$:CO_2 molar ratio from 1:2 to 1:7
181 did not lead to significant changes in the XRD patterns, where nesquehonite continued to be
182 the dominate phase which is consistent with the SEM observation (Fig. 2).
183
184 The "house of cards" morphology is related to a dissolution-recrystallization self-assembly
185 growth mechanism when the dissolution rate of nesquehonite was faster than the precipitation
186 rate of hydromagnesite [52]. Thus, the formation of "house of cards" texture on the surface of
187 HMCs synthesized at $Mg(OH)_2$:CO_2 molar ratio of 1:7 (Fig. 2g) reveals that while
188 nesquehonite is still the dominating phase of the main body (Fig. 3), nesquehonite on the
189 surface was transformed into hydromagnesite phase due to elevated CO_2 concentration.
190

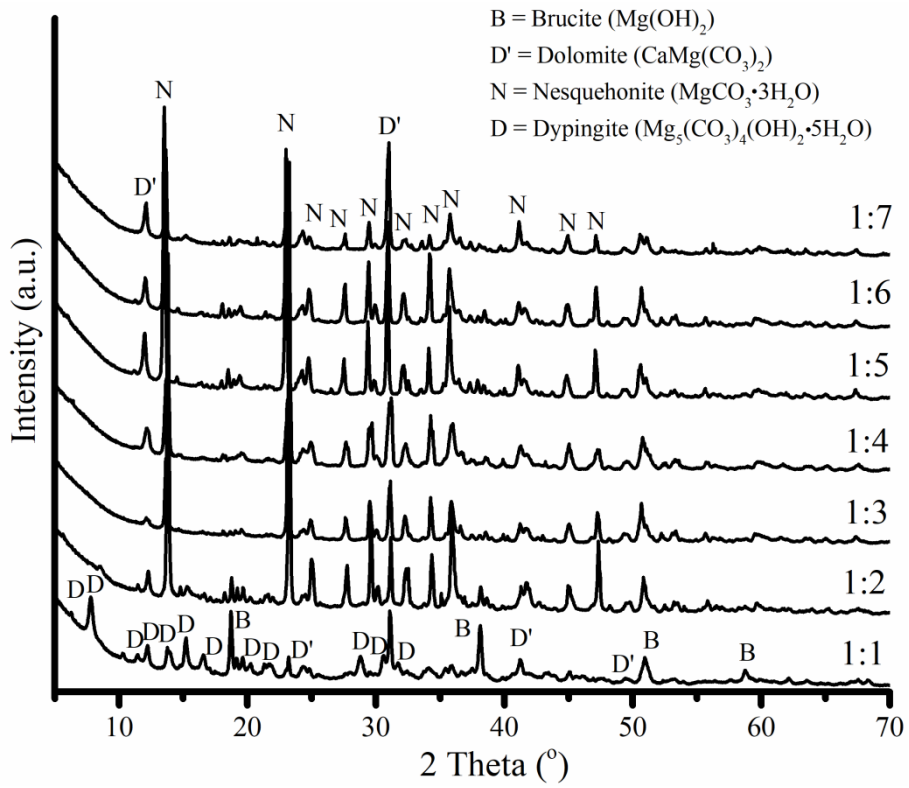

Figure 3 XRD diffractograms of HMCs obtained under a pH of 8 at different $Mg(OH)_2$:CO_2 molar ratios

3.1.2. Effect of pH at $Mg(OH)_2$-to-CO_2 molar ratio of 1

Figure 4 illustrates the FESEM images of the samples obtained under different pH values ranging between 8 and 11, at a constant $Mg(OH)_2$:CO_2 molar ratio of 1:1. At the lower pH values of < 11, the obtained carbonates displayed rosette-like morphologies with an average dimension of ~2 μm, as shown in Figures 4(a)-(c). These rosette-like formations were confirmed to be dypingite, as shown by the XRD patterns presented in Figure 5. As the pH increased from 8 to 10, the intensity of the uncarbonated brucite peak revealed a decrease relative to the others, possibly indicting a reduction in the amount of brucite and an associated higher degree of carbonation at elevated pH levels. This increase in the carbonation degree could be associated with the higher CO_3^{2-}:HCO_3^- ratios in the prepared solutions at elevated pH levels. An increase in the pH led to higher concentrations of OH^-, therefore enabling the

conversion of HCO_3^- to CO_3^{2-}, which then reacted with Mg^{2+}, leading to the precipitation of higher amounts of HMCs in the solution. Alternatively, a further increase in the pH from 11 to 14 lowered the carbonation degree of brucite, which was observed with its flake-like morphology in Figure 4(d). These results were in line with the findings reported in previous studies, where the optimal pH for the carbonation of brucite was shown to be around 9 [53].

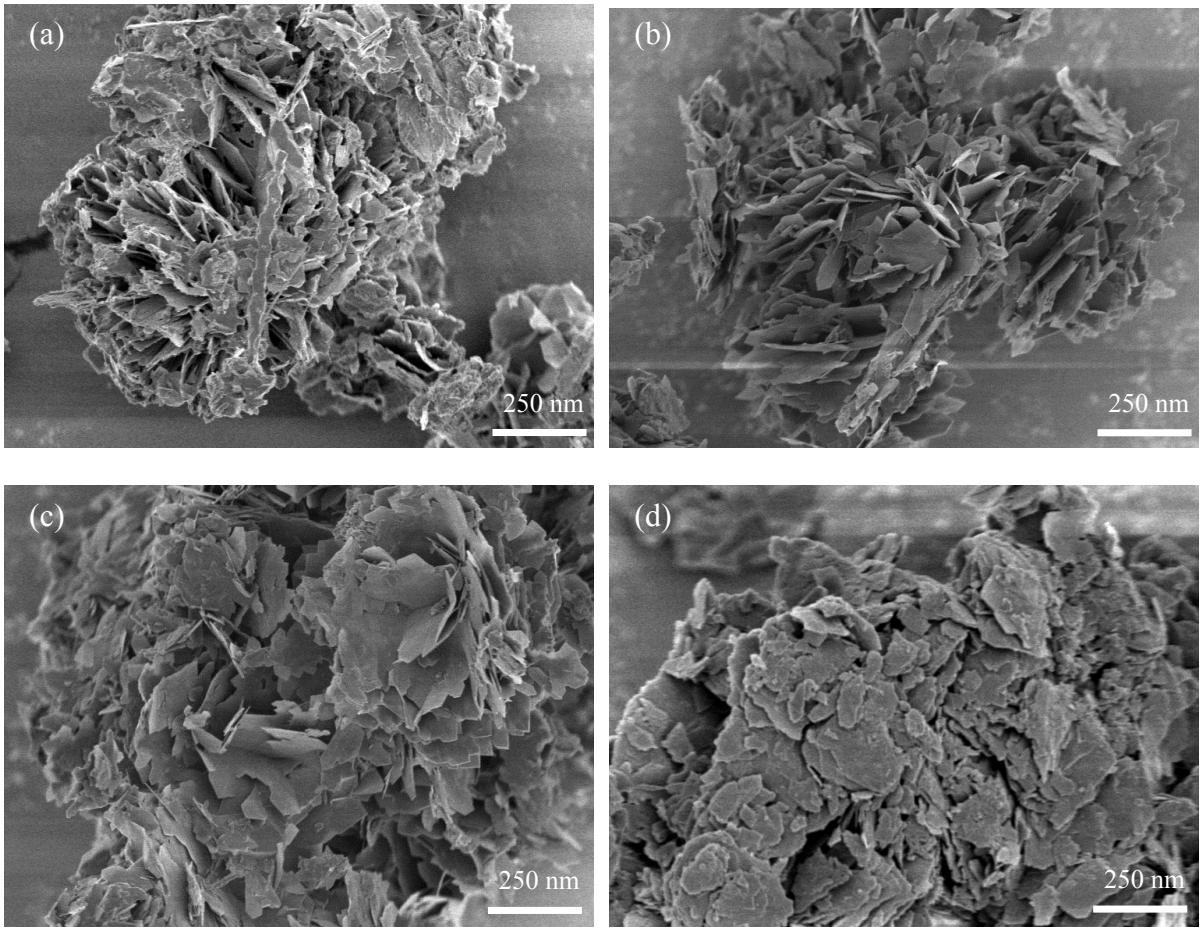

Figure 4 FESEM images of HMCs obtained at the $Mg(OH)_2$:CO_2 molar ratio of 1:1 under different pH values of (a) 8, (b) 9, (c) 10 and (d) 11

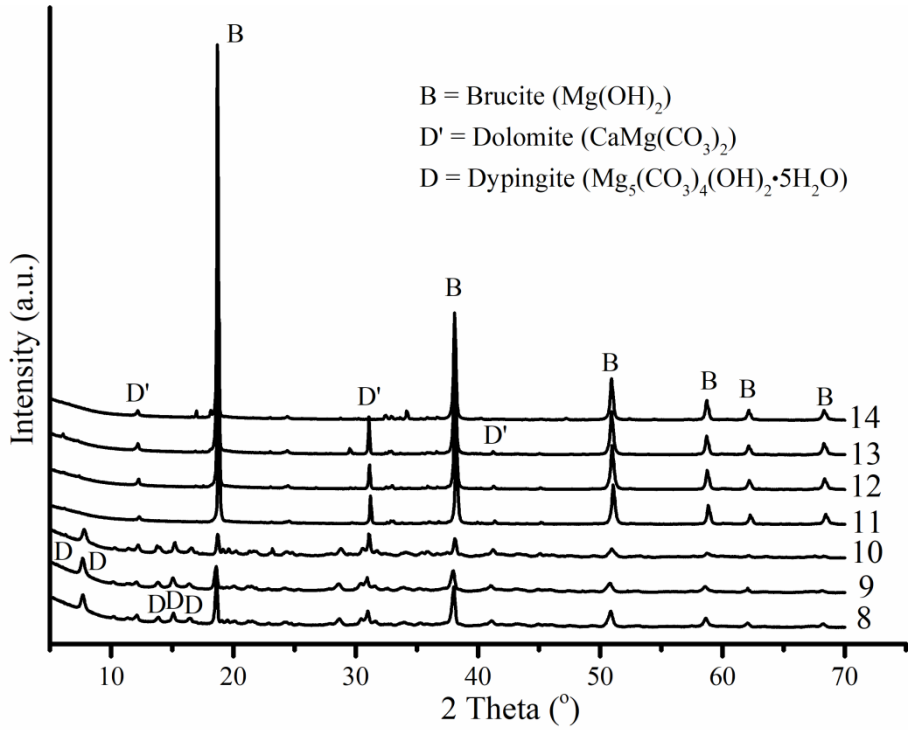

Figure 5 XRD diffractograms of HMCs obtained at the $Mg(OH)_2$:CO_2 molar ratio of 1:1 under different pH values

3.1.3 Effect of pH at $Mg(OH)_2$:CO_2 molar ratio of 1:2

Figure 6 displays the morphologies of HMCs obtained under different pH values at the $Mg(OH)_2$:CO_2 molar ratio of 1:2. Different from HMCs obtained at the $Mg(OH)_2$:CO_2 molar ratio of 1:1, where the presence of dypingite with a rosette-like morphology dominated regardless of the pH value; HMCs obtained at the $Mg(OH)_2$:CO_2 molar ratio of 1:2 clearly demonstrated a different morphology. Instead of the previously observed rosette-like plates, a rod-like structure presenting the "house of cards" texture was seen in samples obtained under pH values of 8 and 9 (Figs. 6a-b). An increase in the pH from 8 onwards resulted in the distortion of the originally clear borders of the nesquehonite crystals, whose shape transformed from the rod-like structure to a cluster of flakes forming on top. This change was mostly obvious at pH values of 10 and 11 (Figures 6(c) and (d)), which revealed the formation of flake-

like clusters with clearly defined boundaries at a pH of 11.

The formation of nesquehonite under pH value of 11 was confirmed by the XRD patterns shown in Figure 7. In line with the findings obtained under the $Mg(OH)_2$:CO_2 molar ratio of 1:1 as revealed in Figure 5, an increase in the pH to 10 and above resulted in the formation of uncarbonated brucite where a flake-like morphology was observed. This "house of cards" texture observed within the prepared samples was attributed to the dissolution-recrystallization-self-assembly growth mechanism as explained in the aforementioned text. The elevated pH used in the experiments conducted in this study increased the solubility of CO_2 in the solution. This has led to a dissolution of the surface of nesquehonite and served as the nucleation points for further hydromagnesite/dypingite plates growing with excessive CO_2 at the surface.

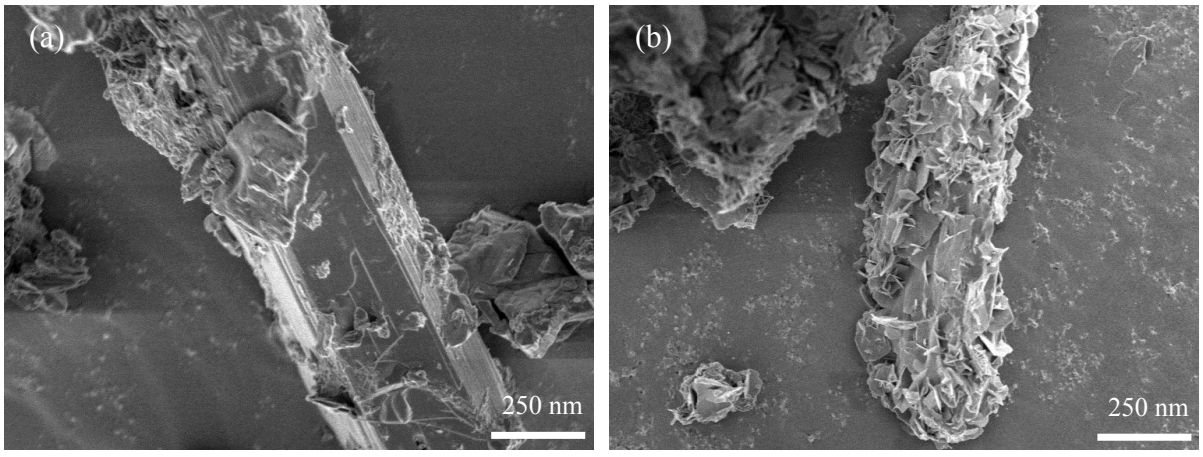

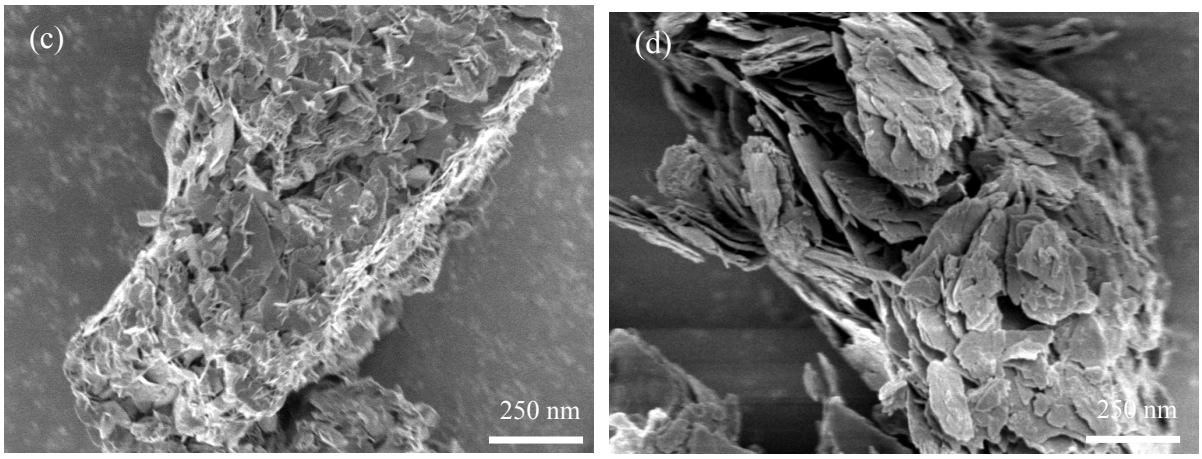

Figure 6 Typical FESEM images of HMCs obtained at a $Mg(OH)_2$:CO_2 molar ratio of 1:2 under different pH values of (a) 8, (b) 9, (c) 10 and (d) 11

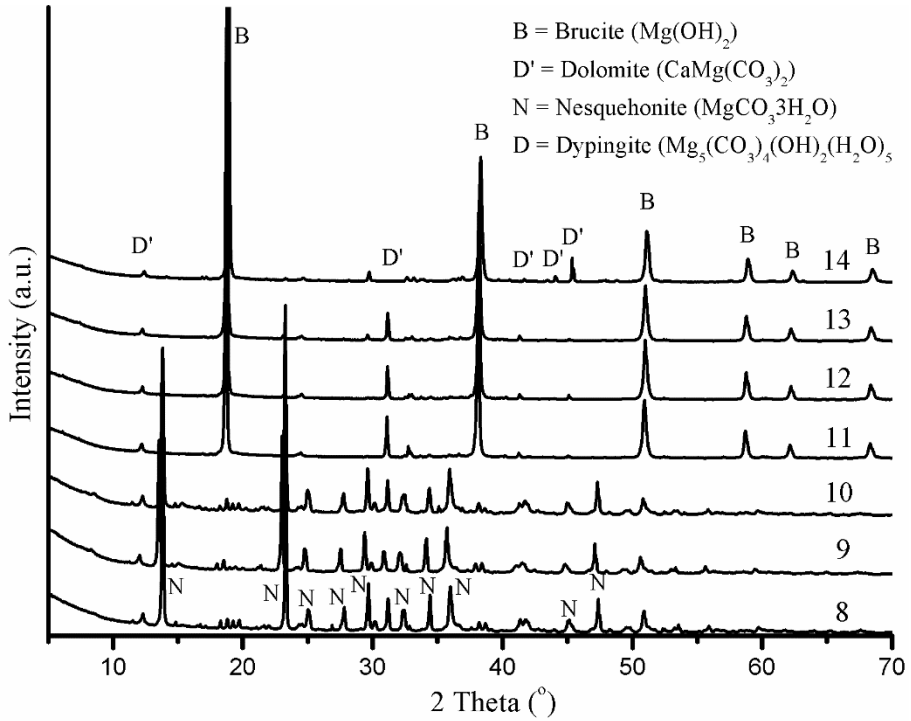

Figure 7 XRD diffractograms of HMCs obtained at the $Mg(OH)_2$:CO_2 molar ratio of 1:2 under different pH values

3.2. Comparison of HMCs synthesized from different source

This section aims to provide a comparison of HMCs obtained via reject brine to those of

chemical $Mg(OH)_2$ slurry, whose detailed characterization was presented earlier in Section 3.1. The findings presented here aim to use reject brine for the long-term storage of anthropogenic CO_2.

3.2.1. Microstructure of HMCs

Figure 8 provides a comparison of the morphologies of HMCs synthesized from $Mg(OH)_2$ slurry and reject brine under a constant pH and $Mg(OH)_2$:CO_2 molar ratio of 8 and 1:1, respectively. As shown in Figure 8(a), the carbonate crystals obtained via the use of $Mg(OH)_2$ slurry led to a rosette-like morphology. Alternatively, the carbonation of reject brine led to the formation of a needle-like morphology with clear boundaries, as seen in Figure 8(b). The compositions of these rosette- and needle-like particles were confirmed to be nesquehonite and dypingite by XRD patterns revealed in Figure 9, respectively. The formation of different Mg-carbonate phases via the two sources could be associated with the relatively higher reactivity of $Mg(OH)_2$ prepared from reject brine when compared to that of $Mg(OH)_2$ slurry (i.e. with a specific surface area of 7.4 vs. 4.8 m^2/g as tested by BET analysis). The carbonation of $Mg(OH)_2$ with a higher reactivity could have capture more CO_2 and enabled the formation of nesquehonite as opposed to dypingite since nesquehonite requires a higher Mg:CO_2 molar ratio as explained in the aforementioned text. This difference in the reactivity of the two samples was also reflected by the absence of the residual brucite peaks in reject brine, as opposed to the clearly defined uncarbonated brucite peaks observed in the $Mg(OH)_2$ slurry, as seen in Figure 9.

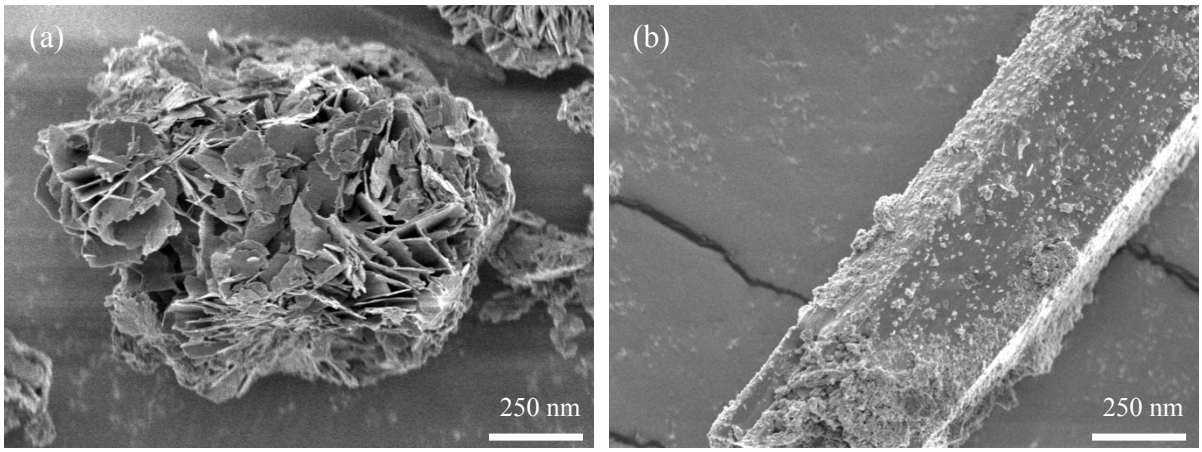

Figure 8 SEM images of HMCs obtained at the $Mg(OH)_2$:CO_2 molar ratio of 1:1 under a pH of 8, showing (a) $Mg(OH)_2$ slurry and (b) reject brine

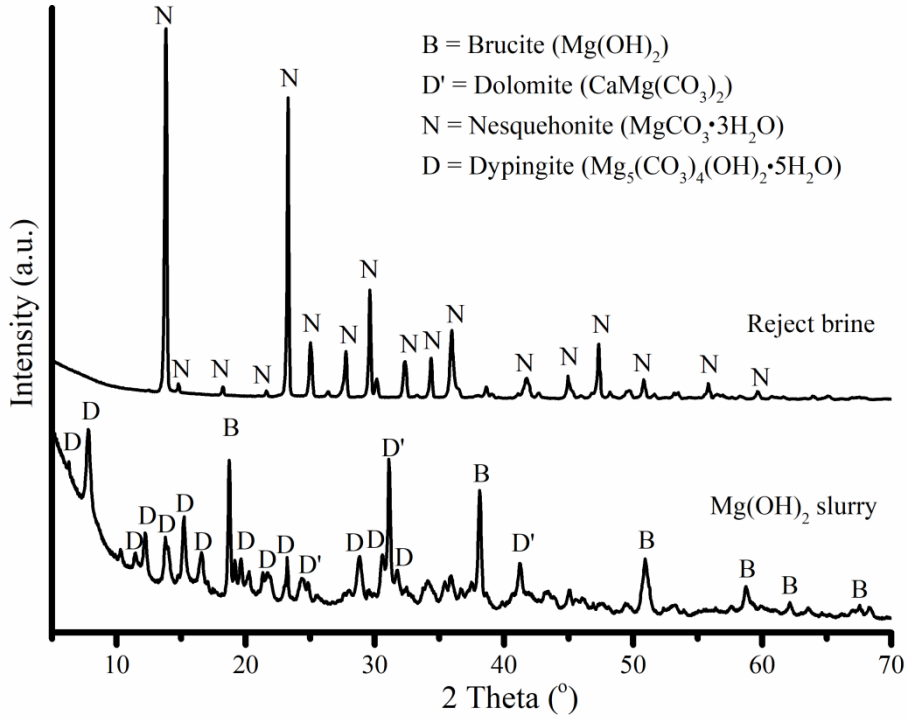

Figure 9 XRD diffractograms of HMCs obtained from $Mg(OH)_2$ slurry and reject brine at the $Mg(OH)_2$:CO_2 molar ratio of 1:1 under a pH of 8

3.2.2. CO_2 capture and storage

The quantitative analysis of the chemical composition of HMCs and amount of CO_2 used in their formation was carried out via TG/DTA and ICP-OES analyses. Figure 10 presents the TG/DTA graphs of HMCs obtained from $Mg(OH)_2$ slurry and reject brine at the $Mg(OH)_2$:CO_2 molar ratio of 1:1 and under a pH 8. Both systems demonstrated a similar trend with three stages of mass loss, which corresponded well with previous studies [36, 54, 55]. Firstly, the dehydration of HMCs took place at ~100-250 °C, resulting in the loss of H_2O. The second mass loss occurred between 250 and 550 °C, which was because of the decomposition of uncarbonated $Mg(OH)_2$ into MgO as well as the decarbonation of HMCs, resulting in a loss of H_2O and CO_2. The final mass loss observed between 550 and 700 °C was due to the decomposition of dolomite and calcite, respectively, which was present as an impurity in the two systems (i.e. in the form of dolomite in $Mg(OH)_2$ slurry and calcite in reject brine).

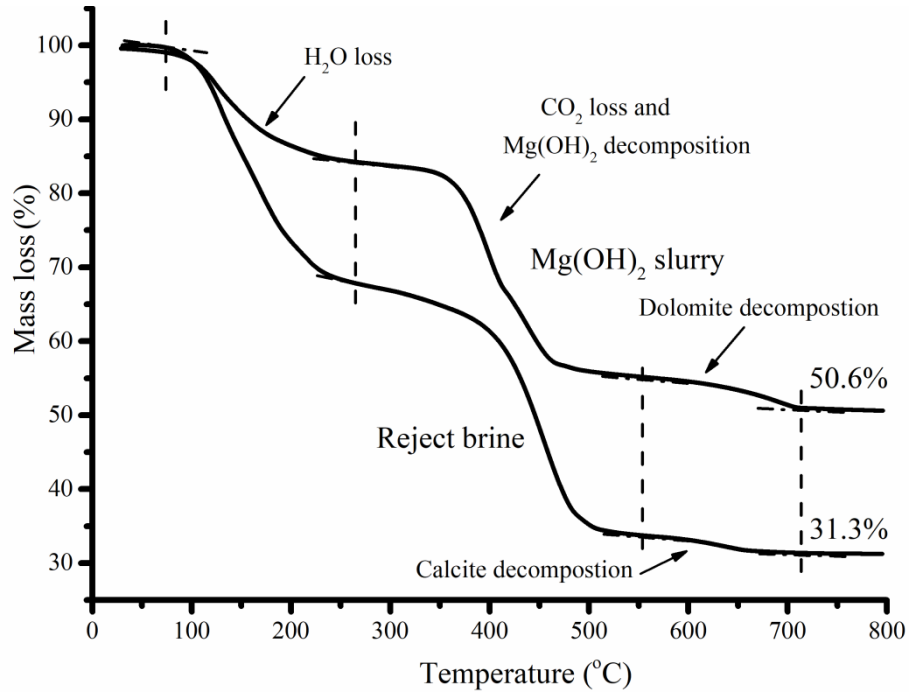

Figure 10 Typical TG/DTA curves of HMCs obtained from $Mg(OH)_2$ slurry and reject brine at the $Mg(OH)_2$:CO_2 molar ratio of 1:1 under a pH of 8

303 The chemical composition of the final product was determined via a combination of the results
304 generated by TG/DTA and ICP-OES, where the recovery rate of Mg^{2+} was measured via ICP-
305 OES and TG/DTA was used to determine the quantity of each phase derived from XRD results.
306 Table 2 revealed the composition of the precipitate synthesized via the carbonation of $Mg(OH)_2$
307 slurry to be composed of 62.1% dypingite and 30.5% uncarbonated brucite. On the other hand,
308 the carbonation of reject brine led to a precipitate composed of 93.1% nesquehonite and 3.7%
309 uncarbonated brucite, as detailed in Table 2. These results were used in the calculation of the
310 percentage of captured CO_2, which was derived by measuring the mass of CO_2 in the HMCs
311 (i.e. dypingite/nesquehonite) divided by the initial input of CO_2 degassed to the system at the
312 $Mg(OH)_2$:CO_2 molar ratio of 1:1. The outcome of these analyses indicated that 43.7% CO_2
313 could be sequestered in the form of dypingite via the defusing CO_2 into $Mg(OH)_2$ slurry, while
314 the corresponding ratio of CO_2 sequestered in reject brine was calculated to be 82.6%. The
315 higher efficiency of CO_2 sequestration achieved via the use of reject brine was associated with
316 the increased reactivity of $Mg(OH)_2$ synthesized from reject brine. Details of the chemical
317 composition and the percentage of captured CO_2 were included in the Appendix section.
318
319 Table 2 Chemical composition of HMCs synthesized from $Mg(OH)_2$ slurry and reject brine at
320 the $Mg(OH)_2$:CO_2 molar ratio of 1:1 under a pH of 8

$Mg(OH)_2$ slurry	Mass (g)	Mass (%)	Reject brine	Mass (g)	Mass (%)
Dypingite	0.6	62.1	Nesquehonite	1.51	93.1
Brucite	0.07	30.5	Brucite	0.06	3.7
Dolomite	0.3	7.4	Calcite	0.05	3.2
CO_2 captured (%)	43.7		CO_2 captured (%)	82.6	

321
322 According to the Paris Agreement, it aims to reduce GHG emissions by 20% (*i.e.,* 7 gigatonnes
323 CO_2 emission reduction as annual anthropogenic CO_2 emissions is about 35 gigatonnes [56])
324 in order to hold the increase in the global average temperature to below 2°C above pre-

industrial levels [56]. According to the International Desalination Association, the global daily production of desalinated water generated by 18,426 desalination plants worldwide exceeds 86.8 million m^3 [47]. It is estimated that an equivalent amount of reject brine is generated [47]. The concentration of Mg^{2+} in reject brine is around 1700 ppm, and thus around 54 million tonnes of Mg could be recovered every year. With a carbon capture and storage rate of 82.6% in the current study, around 45 million tonnes of CO_2 can be sequestrated annually. The suggested methodology thus contributes to around 1% of the required CO_2 emission reduction (*i.e.,* 7 gigatonnes) aimed in the Paris Agreement.

4. Summary and Conclusions

This study presented the influences of key parameters including the $Mg(OH)_2$:CO_2 molar ratio, pH, and $Mg(OH)_2$ source on the synthesis of HMCs through the carbonation of $Mg(OH)_2$ slurry. The resulting HMCs were characterized via a combination of techniques including XRD, FESEM, and TG/DTA. Main conclusions drawn from this study are summarized below.

- The carbonation of $Mg(OH)_2$ slurry under the elevated of $Mg(OH)_2$:CO_2 molar ratio resulted in the transformation of dypingite to nesquehonite.
- Increasing the pH from 8 to 10 was found to promote the carbonation process of $Mg(OH)_2$, resulting in a higher carbonation degree.
- A specific "house of cards" texture, involving the formation of rosette-like dypingite flakes on the surface of nesquehonite needles, was discovered under elevated pH and $Mg(OH)_2$:CO_2 ratios conditions. The formation of this structure was associated with to a dissolution-recrystallization-self-assembly growth mechanism as nesquehonite was seen as a precursor for the further nucleation and seeding of hydromagnesite/dypingite on the surface.

- Carbonation of $Mg(OH)_2$ slurry synthesized from reject brine led to high yield, high purity, and high carbonation degree (82.6%) HMCs. Reject brine shows high potential to be used for capture and long-term storage of CO_2 in the form of HMCs.

The use of compressed commercial CO_2 in the research was to provide a pure source to evaluate CO_2 sequestration rate of the synthesized $Mg(OH)_2$ from desalination reject brine, which served as a model cast study. In the 'real world' case, different CO_2 sources and collecting methods such as CO_2 generated from factories, coal burning power plants, and municipal solid waste incineration plants, may be used. However, further study is necessary to evaluate CO_2 sequestration efficiency of the synthesized $Mg(OH)_2$ with different CO_2 sources and collecting methods. Furthermore, it is necessary to evaluation of the mass, energy, reagents, wastes that come into play in the global process from the life cycle and life cycle cost viewpoint of HMCs synthesized from reject brine.

Acknowledgement

The authors would like to acknowledge the financial support from the Singapore Ministry of Education Academic Research Fund Tier 2 (MOE2017-T2-1-087 (S)) for the completion of this research project.

References

[1] International Energy Agency, Tracking industrial energy efficiency and CO2 emissions, in, Organisation for Economic Co-operation and Development, 2007.

372 [2] V. Mashayekhizadeh, M.H. Ghazanfari, R. Kharrat, M. Dejam, Pore-level observation of
373 free gravity drainage of oil in fractured porous media, Transport in porous media, 87
374 (2011) 561-584.
375 [3] M. Dejam, M.H. Ghazanfari, V. Mashayekhizadeh, M. Kamyab, Factors affecting the
376 gravity drainage mechanism from a single matrix block in naturally fractured reservoirs,
377 Special Topics & Reviews in Porous Media: An International Journal, 2 (2011).
378 [4] M. Dejam, M.H. Ghazanfari, M. Kamyab, M. Masihi, The gas-oil gravity drainage model
379 in a single matrix block: a new relationship between relative permeability and capillary
380 pressure functions, Journal of Porous Media, 14 (2011).
381 [5] V. Mashayekhizadeh, R. Kharrat, M. Ghazanfari, M. Dejam, An experimental
382 investigation of fracture tilt angle effects on frequency and stability of liquid bridges in
383 fractured porous media, Petroleum Science and Technology, 30 (2012) 807-816.
384 [6] M. Dejam, H. Hassanzadeh, Z. Chen, Semi-analytical solutions for a partially penetrated
385 well with wellbore storage and skin effects in a double-porosity system with a gas cap,
386 Transport in porous media, 100 (2013) 159-192.
387 [7] J.D. Figueroa, T. Fout, S. Plasynski, H. McIlvried, R.D. Srivastava, Advancesn in CO2
388 capture technology - the US department of energy's carbon sequestration program, Int. J.
389 Greenh. Gas Control, 2 (2008) 9-20.
390 [8] T. Morita, J. Robinson, A. Adegbulugbe, J. Alcamo, D. Herbert, E.L. La Rovere, N.
391 Nakicenovic, H. Pitcher, P. Raskin, K. Riahi, Greenhouse gas emission mitigation
392 scenarios and implications, Climate Change, (2001) 115-166.
393 [9] P. Forster, V. Ramaswamy, P. Artaxo, T. Berntsen, R. Betts, D.W. Fahey, J. Haywood, J.
394 Lean, D.C. Lowe, G. Myhre, Changes in atmospheric constituents and in radiative
395 forcing. Chapter 2, Climate Change 2007. The Physical Science Basis, (2007).

[10] H. Arakawa, M. Aresta, J.N. Armor, M.A. Barteau, E.J. Beckman, A.T. Bell, J.E. Bercaw, C. Creutz, E. Dinjus, D.A. Dixon, K. Domen, D.L. DuBois, J. Eckert, E. Fujita, D.H. Gibson, W.A. Goddard, D.W. Goodman, J. Keller, G.J. Kubas, H.H. Kung, J.E. Lyons, L.E. Manzer, T.J. Marks, K. Morokuma, K.M. Nicholas, R. Periana, L. Que, J. Rostrup-Nielson, W.M.H. Sachtler, L.D. Schmidt, A. Sen, G.A. Somorjai, P.C. Stair, B.R. Stults, W. Tumas, Catalysis research of relevance to carbon management: Progress, challenges, and opportunities, Chemical Reviews, 101 (2001) 953-996.

[11] R. Lal, Soil carbon sequestration impacts on global climate change and food security, Science, 304 (2004) 1623-1627.

[12] R.S. Haszeldine, Carbon capture and storage: How green can black be?, Science, 325 (2009) 1647-1652.

[13] A.B. Rao, E.S. Rubin, A technical, economic, and environmental assessment of amine-based CO2 capture technology for power plant greenhouse gas control, Environmental Science & Technology, 36 (2002) 4467-4475.

[14] H.J. Herzog, CO2 capture, reuse, and sequestration technologies for mitigating global climate change, in, USDOE Federal Energy Technology Center, Morgantown, WV (United States), 1998.

[15] A. Botha, C.A. Strydom, Preparation of a magnesium hydroxy carbonate from magnesium hydroxide, Hydrometallurgy, 62 (2001) 175-183.

[16] E. Rendek, G. Ducom, P. Germain, Carbon dioxide sequestration in municipal solid waste incinerator (MSWI) bottom ash, Journal of Hazardous Materials, 128 (2006) 73-79.

[17] J.T. Kloprogge, W.N. Martens, L. Nothdurft, L.V. Duong, G.E. Webb, Low temperature synthesis and characterization of nesquehonite, J. Mater. Sci. Lett., 22 (2003) 825-829.

[18] V. Ferrini, C. De Vito, S. Mignardi, Synthesis of nesquehonite by reaction of gaseous CO2 with Mg chloride solution: Its potential role in the sequestration of carbon dioxide, Journal of Hazardous Materials, 168 (2009) 832-837.

[19] E.H. Oelkers, S.R. Gislason, J. Matter, Mineral carbonation of CO2, Elements, 4 (2008) 333-337.

[20] S.J. Gerdemann, W.K. O'Connor, D.C. Dahlin, L.R. Penner, H. Rush, Ex situ aqueous mineral carbonation, Environmental Science & Technology, 41 (2007) 2587-2593.

[21] W.J.J. Huijgen, G.J. Witkamp, R.N.J. Comans, Mineral CO2 sequestration by steel slag carbonation, Environmental Science & Technology, 39 (2005) 9676-9682.

[22] M. Dejam, H. Hassanzadeh, The role of natural fractures of finite double-porosity aquifers on diffusive leakage of brine during geological storage of CO2, Int. J. Greenh. Gas Control, 78 (2018) 177-197.

[23] M. Dejam, H. Hassanzadeh, Diffusive leakage of brine from aquifers during CO2 geological storage, Advances in Water Resources, 111 (2018) 36-57.

[24] M. Hanchen, V. Prigiobbe, R. Baciocchi, M. Mazzotti, Precipitation in the Mg-carbonate system - effects of temperature and CO2 pressure, Chemical Engineering Science, 63 (2008) 1012-1028.

[25] W.K. O'Connor, D.C. Dahlin, G.E. Rush, C.L. Dahlin, W.K. Collins, Carbon dioxide sequestration by direct mineral carbonation: process mineralogy of feed and products, Minerals & Metallurgical Processing, 19 (2002) 95-101.

[26] M.M. Maroto-Valer, D.J. Fauth, M.E. Kuchta, Y. Zhang, J.M. Andrésen, Activation of magnesium rich minerals as carbonation feedstock materials for CO2 sequestration, Fuel Process. Technol., 86 (2005) 1627-1645.

443 [27] A. Sanna, M. Uibu, G. Caramanna, R. Kuusik, M.M. Maroto-Valer, A review of mineral
444 carbonation technologies to sequester CO2, Chemical Society Reviews, 43 (2014) 8049-
445 8080.
446 [28] C. Unluer, A. Al-Tabbaa, Enhancing the carbonation of MgO cement porous blocks
447 through improved curing conditions, Cement and Concrete Research, 59 (2014) 55-65.
448 [29] C. Unluer, A. Al-Tabbaa, Impact of hydrated magnesium carbonate additives on the
449 carbonation of reactive MgO cements, Cement and Concrete Research, 54 (2013) 87-97.
450 [30] M. Liska, A. Al-Tabbaa, K. Carter, J. Fifield, Scaled-up commercial production of
451 reactive magnesia cement pressed masonry units. Part II: Performance, Proceedings of
452 the Institution of Civil Engineers-Construction Materials, 165 (2012b) 225-243.
453 [31] M. Liska, A. Al-Tabbaa, K. Carter, J. Fifield, Scaled-up commercial production of
454 reactive magnesium cement pressed masonry units. Part I: Production, Proceedings of
455 the Institution of Civil Engineers-Construction Materials, 165 (2012a) 211-223.
456 [32] A. Al-Tabbaa, Reactive magnesia cement, Eco-Efficient Concrete, (2013) 523-543.
457 [33] T.J. Wolery, A software package for geochemical modeling of aqueous systems:
458 package overview and installation guide (version 7.0), Lawrence Livermore National
459 Laboratory Livermore, CA, 1992.
460 [34] C. Christ, P. Hostetler, Studies in the system MgO-SiO2-CO2-H2O (II); the activity-
461 product constant of magnesite, American Journal of Science, 268 (1970) 439-453.
462 [35] J. Kittrick, F. Peryea, Determination of the Gibbs free energy of formation of magnesite
463 by solubility methods, Soil Science Society of America Journal, 50 (1986) 243-247.
464 [36] P. Ballirano, C. De Vito, S. Mignardi, V. Ferrini, Phase transitions in the Mg-CO2-H2O
465 system and the thermal decomposition of dypingite, Mg5(CO3)4(OH)2·5H2O:
466 Implications for geosequestration of carbon dioxide, Chemical Geology, 340 (2013) 59-
467 67.

[37] S. Teir, S. Eloneva, C.-J. Fogelholm, R. Zevenhoven, Fixation of carbon dioxide by producing hydromagnesite from serpentinite, Applied Energy, 86 (2009) 214-218.

[38] Y. Wang, Z. Li, G.P. Demopoulos, Controlled precipitation of nesquehonite (MgCO3·3H2O) by the reaction of MgCl2 with (NH4)2CO3, Journal of Crystal Growth, 310 (2008) 1220-1227.

[39] D.K. Panesar, L. Mo, Properties of binary and ternary reactive MgO mortar blends subjected to CO2 curing, Cement and Concrete Composites, 38 (2013) 40-49.

[40] Z. Zhang, Y. Zheng, Y. Ni, Z. Liu, J. Chen, X. Liang, Temperature-and pH-dependent morphology and FT-IR analysis of magnesium carbonate hydrates, The Journal of Physical Chemistry B, 110 (2006) 12969-12973.

[41] L. Hopkinson, P. Kristova, K. Rutt, G. Cressey, Phase transitions in the system MgO-CO2-H2O during CO2 degassing of Mg-bearing solutions, Geochimica Et Cosmochimica Acta, 76 (2012) 1-13.

[42] P. Ballirano, C. De Vito, V. Ferrini, S. Mignardi, The thermal behaviour and structural stability of nesquehonite, MgCO3.3H2O, evaluated by in situ laboratory parallel-beam X-ray powder diffraction: New constraints on CO2 sequestration within minerals, Journal of Hazardous Materials, 178 (2010) 522-528.

[43] S. Adham, A. Hussain, J.M. Matar, R. Dores, A. Janson, Application of Membrane Distillation for desalting brines from thermal desalination plants, Desalination, 314 (2013) 101-108.

[44] S. Mignardi, C. De Vito, V. Ferrini, R.F. Martin, The efficiency of CO2 sequestration via carbonate mineralization with simulated wastewaters of high salinity, Journal of Hazardous Materials, 191 (2011) 49-55.

491 [45] Y. Soong, A.L. Goodman, J.R. McCarthy-Jones, J.P. Baltrus, Experimental and
492 simulation studies on mineral trapping of CO_2 with brine, Energy Conversion and
493 Management, 45 (2004) 1845-1859.
494 [46] Y. Soong, D.L. Fauth, B.H. Howard, J.R. Jones, D.K. Harrison, A.L. Goodman, M.L.
495 Gray, E.A. Frommell, CO2 sequestration with brine solution and fly ashes, Energy
496 Conversion and Management, 47 (2006) 1676-1685.
497 [47] M.H. El-Naas, Reject brine management, Desalination, Trends and Technologies, (2011)
498 237-252.
499 [48] PUB, Desalinated Water, https: // www.pub.gov.sg /watersupply /fournationaltaps
500 /desalinatedwater.
501 [49] H. Dong, E.-H. Yang, C. Unluer, F. Jin, A. Al-Tabbaa, Investigation of the properties of
502 MgO recovered from reject brine obtained from desalination plants, Journal of Cleaner
503 Production, 196 (2018) 100-108.
504 [50] H. Dong, C. Unluer, E.-H. Yang, A. Al-Tabbaa, Recovery of reactive MgO from reject
505 brine via the addition of NaOH, Desalination, 429 (2018) 88-95.
506 [51] H. Dong, C. Unluer, E.-H. Yang, A. Al-Tabbaa, Synthesis of reactive MgO from reject
507 brine via the addition of NH_4OH, Hydrometallurgy, 169 (2017) 165-172.
508 [52] Z.H. Hao, F.L. Du, Synthesis of basic magnesium carbonate microrods with a "house of
509 cards" surface structure using rod-like particle template, Journal of Physics and
510 Chemistry of Solids, 70 (2009) 401-404.
511 [53] D. Wu, B.J. Luo, W. Liu, L.C. Wang, Y. Yao, X.P. Huang, Study on the process
512 optimization for intermediate Magnesium Carbonate Tri-hydrate, Advanced Materials
513 Research, 960 (2014) 199-203.

514 [54] R. Dell, S. Weller, The thermal decomposition of nesquehonite MgCO3· 3H2O and
515 magnesium ammonium carbonate MgCO3·(NH4)2CO3· 4H2O, Transactions of the
516 Faraday Society, 55 (1959) 2203-2220.
517 [55] J. Lanas, J.I. Alvarez, Dolomitic lime: thermal decomposition of nesquehonite,
518 Thermochimica Acta, 421 (2004) 123-132.
519 [56] UNFCCC, The Paris Agreement Conference of the parties to the UNFCCC, (2015).
520
521
522

Appendix – Chemical composition of HMCs and CO_2 captured percentage

HMCs synthesized from $Mg(OH)_2$ slurry

Initially, 0.82 g $Mg(OH)_2$ is added into 200 ml distil water at a $Mg(OH)_2/CO_2$ molar ratio of 1. Assuming a purity of 92% for $Mg(OH)_2$, the remaining 8% impurity is dolomite which does not react or dissolve in the solution. The final precipitates consist of uncarbonated brucite, dypingite and dolomite as supported by XRD results (Figures 5 and 7), which after calcination decompose into MgO, MgO, and CaO·MgO, respectively. Let x and y denote the weights of the uncarbonated brucite and dypingite, respectively. The weight of dolomite is 0.066 g calculated based on 8% of the initial sample weight (i.e., 0.82 g). Residues after the TG/DTA test is 50.6% (Figure 10). Based on the given information, the following equation can be established.

$$\frac{\frac{40}{58}\boldsymbol{x}+\frac{40}{96.8}\boldsymbol{y}+\mathbf{0.82}\times\mathbf{0.08}\times\frac{96}{184}}{\boldsymbol{x}+\boldsymbol{y}+\mathbf{0.82}\times\mathbf{0.08}}=\mathbf{0.506} \quad \text{(A1)}$$

Furthermore, the concentration of Mg^{2+} in the residue was measured to be 308.4 ppm (0.308 g/L) as shown in Table 3. Thus,

$$\frac{\frac{24}{58}x+\frac{24}{96.8}y}{0.2}=\frac{\frac{24}{58}\times 0.82\times 0.92}{0.2}-0.308 \quad \text{(A2)}$$

By solving the two Eqns. (A1) and (A2), the weights of uncarbonated brucite and dypingite are calculated to be 0.27 g and 0.55 g, respectively. The sum of the weights of uncarbonated brucite, dolomite and dypingite was calculated to be 0.89 g, which was higher than 0.46 g of the weighted precipitate as shown in Table 3. This was mainly due to the weight losses during the process of separating the samples from the solution and grinding. The captured CO_2 percentage was calculated by measuring the weight of CO_2 in the HMCs (dypingite) divided by the initial

input of CO_2 degassed to the system at the $Mg(OH)_2/CO_2$ molar ratio of 1, which was calculated to be 43.7% in consideration of 8% impurity.

Table A1 Concentration of Mg^{2+} in the residue and final weight of HMCs obtained from $Mg(OH)_2$ slurry and reject brine

	Mg^{2+} in the residue solution (ppm)	Weight of solids (g)
$Mg(OH)_2$ slurry	309.9 ± 5.2	0.46 ± 0.20
Reject brine	161.5 ± 9.1	1.24 ± 0.14

HMCs synthesized from reject brine

The same principal applies to HMCs synthesized from the reject brine. The $Mg(OH)_2$ sample precipitated from reject brine in the first step contains 6.3% calcite as the impurity which has been detailed in [50]. The XRD result confirms that HMCs after carbonation of $Mg(OH)_2$ consisted of nesquehonite, uncarboned brucite and calcite, which after calcination decompose into **MgO, MgO and CaO**, respectively. Let *x* and *y* denoted the weights of uncarboned brucite and nesquehonite, respectively. The weight of calcite is 0.052 g calculated based on 6.3% of the initial sample weight (i.e., 0.82 g). Residues after the TG/DTA test is 31.3% (Figure 10). Based on the given information, the following equation can be established.

$$\frac{\frac{40}{58}x + \frac{40}{138}y + 0.82 \times 0.063 \times \frac{56}{100}}{x + y + 0.82 \times 0.063} = 0.313 \quad \text{(A3)}$$

Furthermore, the concentration of Mg^{2+} in the residue brine was measured to be 159.3 ppm (0.159 g/L) as shown in Table 3. Thus,

$$\frac{\frac{24}{58}x + \frac{24}{138}y}{0.2} = \frac{\frac{24}{58} \times 0.82 \times 0.937}{0.2} - 0.159 \quad \text{(A4)}$$

By solving the two Eqns. (A1) and (A2), the weights of uncarbonated brucite and nesquehonite are calculated to be 0.06 g and 1.51 g, respectively. The captured CO_2 percentage was calculated by measuring the weight of CO_2 in the HMCs (nesquehonite) divided by the initial

570 input of CO_2 degassed to the system at the $Mg(OH)_2/CO_2$ molar ratio of 1, which was calculated
571 to be 82.6% in consideration of 6.3% impurity. A successful sequestration of CO_2 into reject
572 brine as HMCs was therefore achieved to obtain an efficiency as high as 82.6%, which was
573 significantly improved compared to the $Mg(OH)_2$ slurry.
574